

THE REGULARIZED VISIBLE FOLD REVISITED

K. ULDALL KRISTIANSEN

Department of Applied Mathematics and Computer Science,
Technical University of Denmark,
2800 Kgs. Lyngby,
DK

ABSTRACT. The planar visible fold is a simple singularity in piecewise smooth systems. In this paper, we consider singularly perturbed systems that limit to this piecewise smooth bifurcation as the singular perturbation parameter $\epsilon \rightarrow 0$. Alternatively, these singularly perturbed systems can be thought of as regularizations of their piecewise counterparts. The main contribution of the paper is to demonstrate the use of consecutive blowup transformations in this setting, allowing us to obtain detailed information about a transition map near the fold. We apply this information to prove the existence of a locally unique saddle-node bifurcation in a case where a limit cycle, in the singular limit $\epsilon \rightarrow 0$, grazes the discontinuity set. We apply this result to a mass-spring system on a moving belt described by a Stribeck-type friction law.

1. INTRODUCTION

Piecewise smooth (PWS) differential equations appear in many applications, including problems in mechanics (impact, friction, backlash, free-play, gears, rocking blocks), see also Section 2 below, electronics (switches and diodes, DC/DC converters, $\Sigma - \Delta$ modulators), control engineering (sliding mode control, digital control, optimal control), oceanography (global circulation models), economics (duopolies) and biology (genetic regulatory networks): see [5, 27] for further references. However, PWS models do pose mathematical difficulties because they do not in general define a (classical) dynamical system. In particular, forward uniqueness of solutions cannot always be guaranteed; a prominent example of this is the two-fold in \mathbb{R}^3 , see [4].

Frequently, PWS systems are idealisations of smooth systems with abrupt transitions. It is therefore perhaps natural to view a PWS system as a singular limit of a smooth regularized system. This viewpoint has been adopted by many authors, see e.g. [11, 26, 15, 2, 19, 22, 21, 20], and is useful for resolving the ambiguities associated with PWS systems. In [22], for example, the authors showed that the regularization of the visible-invisible two-fold in \mathbb{R}^3 possesses a forward orbit U that is distinguished amongst all the possible forward orbits leaving the two-fold as $\epsilon \rightarrow 0$. Although the details were only given for one particular regularization function (arctan), the authors acknowledged that the results could be extended to other functions (including ones like those in (A1) and (A2) below) without essential changes to their result. The authors used successive blowups to obtain this result. The blowup method, pioneered by Dumortier and Roussarie [6], has in general proven very successful in the geometric analysis of singular perturbation problems

[23, 16, 17, 18]. In this paper, we adopt a similar approach to revisit the planar visible fold and obtain a detailed description of this system.

1.1. Setting. In this paper, we consider planar singularly perturbed systems of the following form

$$\dot{z} = Z(z, \phi(y\epsilon^{-1}, \epsilon), \alpha), \quad (1.1)$$

where $z = (x, y) \in \mathbb{R}^2$ and $\phi : \mathbb{R} \times [0, \epsilon_0] \rightarrow \mathbb{R}$. Moreover, $\epsilon \in [0, \epsilon_0]$ and $\alpha \in I \subset \mathbb{R}$ are parameters and $Z : \mathbb{R}^2 \times \mathbb{R} \times I \rightarrow \mathbb{R}^2$ is smooth in all arguments. Specifically, we will assume that:

(A0) $p \mapsto Z(z, p, \alpha)$ is affine:

$$Z(z, p, \alpha) = pZ_+(z, \alpha) + (1 - p)Z_-(z, \alpha), \quad (1.2)$$

with $Z_{\pm} : \mathbb{R}^2 \times I \rightarrow \mathbb{R}^2$ each smooth.

Regarding the functions ϕ we suppose the following:

(A1) $\phi : \mathbb{R} \times [0, \epsilon_0] \rightarrow \mathbb{R}$ is a smooth “regularization function” satisfying:

$$\phi'_s(s, \epsilon) \equiv \frac{\partial \phi(s, \epsilon)}{\partial s} > 0, \quad (1.3)$$

for all $s \in \mathbb{R}$, $\epsilon \in [0, \epsilon_0]$ and

$$\phi(s, \epsilon) \rightarrow \begin{cases} 1 & \text{for } s \rightarrow \infty \\ 0 & \text{for } s \rightarrow -\infty \end{cases}, \quad (1.4)$$

for each $\epsilon \in [0, \epsilon_0]$. See also Section 5.

(A2) Moreover, there exists $k_{\pm} \in \mathbb{N}$, constants $c_j > 0, j = 0, \dots, 3$ and smooth functions $\phi_{\pm} : [0, c_0] \times [0, c_1] \rightarrow [c_2, c_3]$ such that

$$\begin{aligned} \phi(\epsilon_1^{-1}, r_1\epsilon_1) &= 1 - \epsilon_1^{k_+} \phi_+(\epsilon_1, r_1) \\ \phi(-\epsilon_3^{-1}, r_3\epsilon_3) &= \epsilon_3^{k_-} \phi_-(\epsilon_3, r_3), \end{aligned}$$

for all $(\epsilon_i, r_i) \in [0, c_0] \times [0, c_1]$ and $i = 1, 3$.

In this paper, smooth will be mean C^l with l sufficiently large. We will leave it to the reader to determine what “sufficiently” is for the various statements to come.

Under assumption (A1), $\phi(\cdot, \epsilon)$ is a monotone, switch-like function, and by (A2), fixing $|y| \geq c > 0$, say, (1.1) is regularly perturbed as $\epsilon \rightarrow 0$. However, $y = \epsilon = 0$ is singular for (1.1). But the system does not fit within the framework of Fenichel’s geometric theory of slow-fast systems [7, 8, 9, 14]. In such systems, there is a manifold of equilibria for $\epsilon = 0$. For (1.1), instead the $\epsilon \rightarrow 0$ limit is a piecewise smooth (PWS, henceforth) system

$$\dot{z} = \begin{cases} Z_+(z, \alpha) & \text{for } y > 0, \\ Z_-(z, \alpha) & \text{for } y < 0. \end{cases} \quad (1.5)$$

Nevertheless, we will see, under the assumption (A0), that it is possible to obtain a geometric theory of (1.1) as $\epsilon \rightarrow 0$ using blowup, see also [26, 19, 22].

Along the discontinuity set $\Sigma = \{(x, y) | y = 0\}$, also called the switching manifold in the PWS literature [5], Z_{\pm} can either (a) be pointing in the same directions, (b) be pointing in opposite directions, or at least one of Z_{\pm} is tangent. The subset Σ_{cr} along which (a) occurs is called crossing, which is relatively “harmless”. Here orbits of (1.1) follow the orbits of (1.5) obtained by gluing orbits together on either side. The subset Σ_{sl} along which (b) occurs, on the other hand, is called sliding.

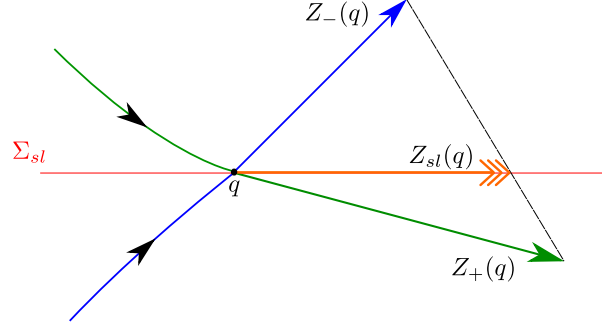


FIGURE 1. Geometric construction of the Filippov sliding vector-field Z_{sl} as the convex combination of Z_{\pm} such that Z_{sl} is tangent to Σ .

Here solutions of (1.5) cannot be extended beyond the intersection with Σ . In the PWS literature, (1.5) is therefore frequently “closed” by subscribing a Filippov vector-field along Σ . See Fig. 1.1 for a geometric construction. Interestingly, under assumption (A0), see [26, 2, 19, 22], the Filippov vector-field also coincides with a reduced vector-field on a critical manifold of (1.1) for $\epsilon = 0$, obtained upon blowup of Σ .

It is possible to characterize crossing and sliding using the Lie derivative $Z_+f(\cdot) = \nabla f(\cdot) \cdot Z_+(\cdot, \alpha)$ of $f(x, y) = y$, such that $\Sigma = \{f(x, y) = 0\}$, along Z_{\pm} :

$$\Sigma_{cr} = \{q \in \Sigma | (Z_+f(q))(Z_-f(q)) > 0\},$$

$$\Sigma_{sl} = \{q \in \Sigma | (Z_+f(q))(Z_-f(q)) < 0\}.$$

In between, are the tangencies

$$T = \{q \in \Sigma | (Z_+f(q))(Z_-f(q)) = 0\}.$$

1.2. The visible fold tangency. In [2], the authors also considered systems of the form (1.1) satisfying (A0). In particular, they considered the local behaviour near a visible fold tangency T , assuming that an orbit γ of Z_+ had a quadratic tangency with Σ at a point $q \in \Sigma$, while $Z_-(q)$ was transverse to Σ . See Fig. 2 for an illustration of the setting. Notice, the tangency is called visible because the orbit γ is contained within $y \geq 0$. Using Lie derivatives, such a visible fold point can be written as

$$Z_+f(q) = 0, Z_+(Z_+f)(q) > 0, Z_-f(q) > 0.$$

Based on appropriate scalings, nonlinear transformations of time and the flow-box theorem, the authors of [2] constructed a change of coordinates such that near q the system could be brought into the form (1.2) with

$$Z_+(z) = \begin{pmatrix} 1 + f(z) \\ 2x + yg(z) \end{pmatrix}, \quad Z_-(z) = \begin{pmatrix} 0 \\ 1 \end{pmatrix} \quad (1.6)$$

where f and g are smooth and where $f(0) = 0$ and $q = (0, 0)$ in the new coordinates, suppressing any dependency on a parameter α in these expressions. The result is local, so we assume $z \in U_\xi \equiv [-\xi, \xi]^2$ with $\xi > 0$ sufficiently small. See [2, Theorem 2]. Setting $f = g = 0$ in (1.6), we realize that the orbit γ , which is tangent to Σ at $(x, y) = (0, 0)$, is close to the parabola $y = x^2$. In any case, it is locally a graph $y = \gamma(x)$, abusing notation slightly. It acts as a separatrix: Everything within $\{(x, y) \in U_\xi | x < 0, 0 < y < \gamma(x)\}$ reaches $y = 0$ and “slides”, whereas everything above $y = \gamma(x)$ does not. See Fig. 2.

The authors of [2] analyse (1.1) with Z_\pm as in (1.6) using asymptotic methods, but considered, following [29], a special class of non-analytic regularization functions $\psi(s)$, independent of ϵ , of the following form:

$$\psi'(s) > 0, \quad \text{for all } s \in (-1, 1),$$

and

$$\begin{aligned} \psi(s) &= 0, & \text{for all } s \leq -1, \\ \psi(s) &= 1, & \text{for all } s \geq 1. \end{aligned} \tag{1.7}$$

Notice that these functions are not asymptotic to 0 and 1 but rather reach these values at finite values of s . Simple functions like $\frac{1}{2} + \frac{1}{\pi} \arctan(s)$ therefore do not belong to this class and in practice (I believe that) any function of this type is piecewise polynomial, the simplest example being

$$\psi(s) = \begin{cases} 1 & \text{for } s \geq 1, \\ \frac{1}{2}s + \frac{1}{2} & \text{for } s \in (-1, 1), \\ 0 & \text{for } s \leq -1, \end{cases}$$

although this is clearly only C^0 . The authors described the perturbation of a critical manifold and its extension by the forward flow into $y > 0$ as $\epsilon \rightarrow 0$ for this class of functions. They also studied the case where an unstable limit cycle of Z_+ grazes Σ and argued that this PWS bifurcation had to give rise to a saddle-node bifurcation of limit cycles for $\epsilon \ll 1$. But they did not proof this statement nor did they address the question of whether additional saddle-nodes could exist.

1.3. Main results. In this paper, we will, following [2, Theorem 2] and the equations (1.6), revisit the results of [2] within our slightly more general framework and demonstrate the use of the successive blowups, also used in [19, 22], to desingularize (1.2).

A local transition map. Let Σ_L and Σ_R be two sections transverse to Z_+ within $y = \delta \in (0, \xi)$ such that points in Σ_L flow to points in Σ_R in finite time by following the flow of Z_+ . Specifically, we take

$$\begin{aligned} \Sigma_L &= \{(x, y) | y = \delta, x \in I_L \subset (-\xi, 0)\}, \\ \Sigma_R &= \{(x, y) | y = \delta, x \in I_R \subset (0, \xi)\}, \end{aligned}$$

where I_L and I_R are closed intervals. By adjusting δ , ξ , I_L and I_R , if necessary, we may assume that γ intersects Σ_L and Σ_R in their interior and that the x -values of the intersection, γ_L and γ_R , respectively, satisfy $\gamma_L < 0 < \gamma_R$. See Fig. 2. Then we define $Q(\cdot, \epsilon)$ as the mapping $I_L \ni x \mapsto Q(x, \epsilon) \in I_R$ obtained by the first

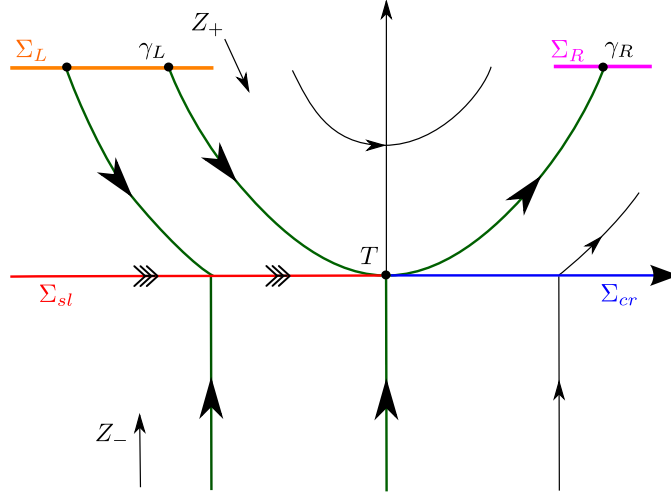


FIGURE 2. The visible fold. Z_+ has a quadratic tangency with Σ at $(x, y) = (0, 0)$ while $Z_-(0, 0)$ is transverse.

intersection of the forward flow of (1.2), with Z_{\pm} as in (1.6). Since k_- plays little role, recall (A2), we set

$$k = k_+,$$

for simplicity in the following.

Theorem 1.1. *Consider (1.1), satisfying (A0), specifically (1.2) with (1.6), and suppose (A1) and (A2).*

- (a) *Fix any $0 < \nu < \xi$ and let $J = [-\xi, -\nu]$. Then there exists an $\epsilon_0 > 0$ such that for any $\epsilon \in (0, \epsilon_0)$, there exists a locally invariant manifold S_{ϵ} as a graph over J :*

$$S_{\epsilon} : y = \epsilon h(x, \epsilon), x \in J,$$

where h is smooth in both variables. The manifold has an invariant Lipschitz foliation of stable fibers along which orbits contract exponentially towards S_{ϵ} . For $\epsilon = 0$ these fibers coincide with the orbits of Z_{\pm} reaching $\Sigma \cap \{x \in J\}$ after a finite time. Moreover, $Z|_{S_{\epsilon}}$ is a regular perturbation of the Filippov vector-field.

- (b) *The forward flow of S_{ϵ} intersects Σ_R in $(m(\epsilon), \delta)$ where*

$$m(\epsilon) = \gamma_R + \epsilon^{2k/(2k+1)} m_1(\epsilon),$$

with m_1 continuous.

- (c) *Fix $\theta > 0$ so small that $0 < \theta - \gamma_L < \xi$ and let $K = [-\xi, \gamma_L - \theta] \subset I_L$. Consider $Q_K(\cdot, \epsilon) = Q(\cdot, \epsilon)|_K : K \rightarrow I_R$. Then Q_K is a strong contraction:*

$$Q_K(x, \epsilon) = m(\epsilon) + \mathcal{O}(e^{-c/\epsilon}), \quad \partial_x Q_K(x, \epsilon) = \mathcal{O}(e^{-c/\epsilon}).$$

- (d) *For any $c > 0$ sufficiently small, there exist positive numbers ϵ_0, δ, ξ , and intervals I_L and I_R such that*

$$(i) \quad |Q'_x(x, \epsilon)| \leq c \text{ for all } x \in I_L \cap \{x \leq \gamma_L - c^{-1} \epsilon^{2k/(2k+1)}\};$$

- (ii) $Q'_x(x, \epsilon) < 0$, $Q''_{xx}(x, \epsilon) < 0$ for all $x \in I_L \cap \{|x - \gamma_L| \leq c^{-1}\epsilon^{2k/(2k+1)}\}$;
 - (iii) $1 - c \leq |Q'_x(x, \epsilon)| \leq 1 + c$ for all $x \in I_L \cap \{x \geq \gamma_L + c^{-1}\epsilon^{2k/(2k+1)}\}$;
- for all $0 < \epsilon \leq \epsilon_0$.

Remark 1.2. Notice, it is possible to obtain a “singular” map $Q_0 : \Sigma_L \rightarrow \Sigma_R$ of the PWS Filippov system. This mapping is of the following form

- (i) $Q'_{0,x}(x) = 0$ for all $x < \gamma_L$;
- (ii) $Q'_{0,x}$ not defined for $x = \gamma_L$;
- (iii) $1 - c \leq |Q'_x(x, \epsilon)| \leq 1 + c$ for all $x > \gamma_L$.

Compare with Theorem 1.1(d). (i) is due to the fact that every point in I_L with $x < \gamma_L$ reaches the sliding segment, see Fig. 2. Hence:

$$Q_0(x) = \gamma_R,$$

for all $x < \gamma_L$.

Application to a grazing bifurcation. We now assume the following:

- (B1) Suppose that Z_+ has a hyperbolic and unstable limit cycle Γ_0 for $\alpha = 0$ with a unique quadratic tangency with $\Sigma = \{y = 0\}$ at the point $q = (0, 0)$.

Since Γ_0 is hyperbolic there exists a local family $\{\Gamma_\alpha\}_{\alpha \in I}$, where

$$I = (-a, a), \quad a > 0, \tag{1.8}$$

of hyperbolic and unstable limit cycles.

- (B2) Let $Y(\alpha) = \min y(t)$ along Γ_α so that $Y(0) = 0$ by assumption (B1). Suppose that

$$Y'(0) > 0.$$

By (B1) and (B2) and the implicit function theorem, Γ_α therefore, for $a > 0$ sufficiently small, recall (1.8), intersects $\{y = 0\}$ only for $\alpha \leq 0$, doing so twice for $\alpha < 0$ and once for $\alpha = 0$. Finally:

- (B3) Suppose that Z_- has a positive y -component at $(x, y) = (0, 0)$ for $\alpha = 0$, i.e. $Z_- f(0, 0) > 0$.

We illustrate the setting in Fig. 3. As a consequence of (B1) and (B3), and the implicit function theorem, the PWS system (Z_-, Z_+) has a visible fold near $(x, y) = (0, 0)$ for all $\alpha \in I$ (after possibly restricting $a > 0$ further). In fact, also by the implicit function theorem, the x -value of this fold point depends smoothly on α and we can therefore shift it to $(x, y) = (0, 0)$ for all α . Moreover, applying the result of [2] we can bring the PWS system into the form (1.6). We will now study the bifurcation of limit cycles that occur for (1.2) near $\alpha = 0$ for all $0 < \epsilon \ll 1$. (In the PWS setting, this bifurcation is known as the grazing bifurcation, see e.g. [25, Fig. 14, section 4.11].) For this we study the Poincaré mapping $P(\cdot, \epsilon, \alpha) : I_R \rightarrow I_R$ obtained by the forward flow. This mapping is well-defined by the assumptions (B1)-(B3) and by Theorem 1.1, based on assumptions (A1)-(A2). We compose

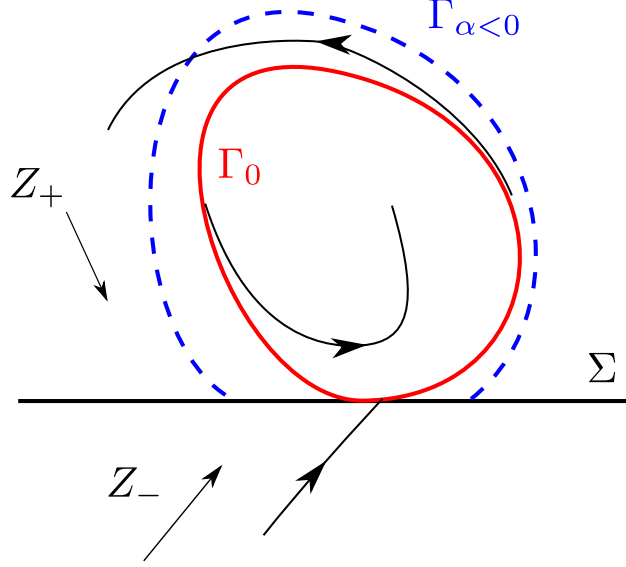


FIGURE 3. A grazing limit cycle for $\alpha = \epsilon = 0$. Assumption (B1) is so that Γ_0 is unstable for Z_+ for $\alpha = 0$. By (B2), $\Gamma_{\alpha < 0}$ (in blue) locally intersects Σ twice near the fold. Black orbits are (backwards) transients for $\alpha = 0$, demonstrating the unstable nature of Γ_0 .

$P(\cdot, \epsilon, \alpha)$ into two parts: A “global” mapping $R(\cdot, \epsilon, \alpha) : I_R \rightarrow I_L$ and the “local” mapping $Q(\cdot, \epsilon, \alpha) : I_L \rightarrow I_R$, studied in Theorem 1.1:

$$P(x, \epsilon, \alpha) = Q(R(x, \epsilon, \alpha), \epsilon, \alpha). \quad (1.9)$$

By (A2), $x \mapsto R(x, \epsilon, \alpha)$ is a regular perturbation of the associated mapping $x \mapsto R(x, 0, \alpha)$ obtain from the Z_+ system.

Lemma 1.3. *Assume (B1) and (B2). The mapping R is smooth in all of its arguments. Also there exists a $\omega > 0$ such that upon decreasing ξ and δ , if necessary, the map satisfies:*

$$R(\gamma_R, 0, 0) = \gamma_L, \quad (1.10)$$

$$R'_x(\gamma_R, 0, 0) < -1 - \omega, \quad (1.11)$$

$$R'_\alpha(\gamma_R, 0, 0) > 0. \quad (1.12)$$

Proof. (1.10) holds by assumption (B1) and the definition of γ_L and γ_R . By (B1), Γ_0 is a hyperbolic but unstable limit cycle of Z_+ . Therefore $P'_x(\gamma_R, 0, 0) > 1$, as a mapping obtained from Z_+ at $\epsilon = 0$ only, and hence by decomposing P into R and Q , we obtain, upon restricting ξ and δ , that $-Q$ is as close to the identity as desired. Indeed, as a mapping obtained from the flow of Z_+ , Q is regular and obtained by a short integration time. The integration time can be decreased by decreasing δ . By the chain rule, we therefore obtain (1.11). Finally, (1.12) follows from (B2). We leave out the simple details. \square

We now have

Theorem 1.4. *Suppose (A0)-(A2) and (B1)-(B3). Then there exists a locally unique saddle-node bifurcation of limit cycles for all $0 < \epsilon \ll 1$ at*

$$\alpha = \epsilon^{2k/(2k+1)} \alpha_1(\epsilon),$$

with α_1 continuous, such that limit cycles only exist within $\alpha \in I$ for $\alpha \leq \epsilon^{2k/(2k+1)} \alpha_1(\epsilon)$, two for $\alpha < \epsilon^{2k/(2k+1)} \alpha_1(\epsilon)$ and precisely one for $\alpha = \epsilon^{2k/(2k+1)} \alpha_1(\epsilon)$. The saddle-node periodic orbit for $\alpha = \epsilon^{2k/(2k+1)} \alpha_1(\epsilon)$ converges in Hausdorff distance to the grazing limit cycle Γ_0 of Z_+ as $\epsilon \rightarrow 0$.

1.4. Overview. In Section 2 we present an example where Theorem 1.4 can be applied and provide some numerical comparisons. We prove Theorem 1.1 in Section 3 and Theorem 1.4 in Section 4. We conclude the paper in Section 5. Here we discuss the assumptions, the regularization functions used, possible extensions to our work and compare our results with [2].

2. THE FRICTION OSCILLATOR

Systems of the form (1.1) often appear in models of friction. Consider for example the system in Fig. 4(a), where a mass-spring system is on a moving belt. This produces the following equations

$$\begin{aligned} \dot{x} &= y - \alpha, \\ \dot{y} &= -x - \mu(y, \phi(y\epsilon^{-1}, \epsilon)), \end{aligned} \tag{2.1}$$

where $\alpha > 0$ is the belt speed, x is the elongation of the spring and y is the velocity relative to the belt, all in nondimensional form. Furthermore, μ is the friction force opposing the relative velocity, i.e. $\mu > 0$ for $y > 0$ and $\mu < 0$ for $y < 0$. Many different forms of μ exists, often PWS, but we will suppose that

$$\mu(y, p) = \mu_+(y)p - \mu_+(-y)(1 - p), \tag{2.2}$$

as desired, such that μ is odd with respect to $(y, p) \mapsto (-y, 1 - p)$. Here $\mu_+(y)$ is smooth function having a minimum at $y = y_0 > 0$, see Fig. 4(b), such that

$$\mu'_+(y_0) = 0, \mu''_+(y_0) > 0, \tag{2.3}$$

and $\mu'_+(y) < 0$ for all $y \in [0, y_0]$ while $\mu'_+(y) > 0$ for all $y \in (y_0, \infty)$. The resulting shape of μ_+ is shown in Fig. 4(b); the initial negative slope is known as the Stribeck effect of friction, see e.g. [1]. In this way, we obtain the following associated PWS system

$$\begin{aligned} Z_+(x, y, \alpha) &= \begin{pmatrix} y - \alpha \\ -x - \mu_+(y) \end{pmatrix}, \\ Z_-(x, y, \alpha) &= \begin{pmatrix} y - \alpha \\ -x + \mu_+(-y) \end{pmatrix}. \end{aligned} \tag{2.4}$$

The system (2.2) with $p = \phi(y/\epsilon, \epsilon)$, ϕ satisfying (A1) and (A2), can viewed as a regularization of the PWS model (Z_+, Z_-) with the PWS friction law

$$\mu(y) = \begin{cases} \mu_+(y) & \text{for } y > 0, \\ -\mu_+(-y) & \text{for } y < 0. \end{cases}$$

Consider now Z_+ . By (2.3), this system clearly has a Hopf bifurcation for $\alpha = y_0$ at $(x, y) = (-\mu_+(y_0), y_0)$. A straightforward calculation also shows that the

Lyapunov coefficient is proportional to $\mu_+'''(y_0)$; the bifurcation being supercritical (subcritical) for $\mu_+'''(y_0) < 0$ ($\mu_+'''(y_0) > 0$, respectively). Suppose the former. Then for y_0 sufficiently small, it follows that the unstable Hopf limit cycles of Z_+ for $\epsilon = 0$ intersect the switching manifold $y = 0$ in the way described in (B1)-(B2) for some value of $\alpha = \alpha_* > y_0$ near y_0 . The fact that $\alpha_* > y_0$ is due to the fact that the limit cycles are unstable. Furthermore, the visible fold tangency with $y = 0$ for $\alpha = \alpha_*$ occurs at the point $q : (x, y) = (-\mu_+(0), 0)$. To verify (B3), notice by (2.4) that $\dot{y} = 2\mu_+(0) > 0$ at q from below. As a result, assuming (A1) and (A2), there exists saddle-node bifurcation of limit cycles near $\alpha = \alpha_*$ for $\epsilon \ll 1$, see Theorem 1.4. We collect the result in the following corollary.

Corollary 2.1. *Consider (2.1) with μ of the form (2.2), where there exists an $y_0 > 0$ such that (2.3) holds and suppose that the regularization function ϕ satisfies (A1)-(A2). Suppose also that $\mu_+'''(y_0) < 0$. Then for y_0 sufficiently small there exists an $\epsilon_0 > 0$ such that for every $\epsilon \in (0, \epsilon_0)$ the following holds:*

- (1) *The exists a supercritical Hopf bifurcation at $\alpha_H(\epsilon) = y_0 + \mathcal{O}(\epsilon)$.*
- (2) *The unstable Hopf limit cycles undergoes a locally unique saddle-node bifurcation at $\alpha_{SN}(\epsilon) = \alpha_* + \epsilon^{2k/(2k+1)}\alpha_1(\epsilon) > \alpha_H(\epsilon)$.*
- (3) *For any $\alpha \in (\alpha_H(\epsilon), \alpha_{SN}(\epsilon))$ two (and, locally, only two) limit cycles exist: $\Gamma_{sl}(\alpha, \epsilon)$ and $\Gamma_+(\alpha, \epsilon)$, where:*
 - Γ_{sl} *is hyperbolic and attracting.*
 - $\lim_{\epsilon \rightarrow 0} \Gamma_{sl}(\alpha, \epsilon)$ *has a sliding segment.*
 - Γ_+ *is hyperbolic and repelling.*
 - $\lim_{\epsilon \rightarrow 0} \Gamma_+(\alpha, \epsilon)$ *is a limit cycle of Z_+ contained within $y > 0$.**No limit cycles exist near $(x, y) = (-\mu_+(y_0), y_0)$ for $\alpha > \alpha_{SN}(\epsilon)$.*
- (4) *Let $\Gamma_{SN}(\epsilon)$ be the saddle-node periodic orbit for $\alpha = \alpha_{SN}(\epsilon)$. Then $\Gamma_{SN}(\epsilon)$ converges in Hausdorff-distance to the unstable limit cycle of Z_+ which grazes $y = 0$ for $\alpha = \alpha_*$.*

Proof. (1) and (2) follows from the analysis preceeding the corollary. (3) and (4) are also a consequences of the proof of Theorem 1.4, recall also Remark 1.2. \square

It is known from experiments that supercritical Hopf bicurcations does occur for certain friction characteristics, see e.g. [12]. Explicitly, it does occur for the model

$$\mu_+(y) = \mu_m + (\mu_s - \mu_m)e^{-\rho y} + cy, \quad (2.5)$$

proposed in [1] and also studied in [30], which we will now use in numerical computations. For (2.5), $\mu_+(0) = \mu_s$ and $\mu_s > \mu_m > 0$, $\rho > 0$, and $c \in (0, \rho(\mu_s - \mu_m))$ for the Stribeck effect and the existence of y_0 to be present. In fact, for (2.5),

$$y_0 = -\rho^{-1} \log(c/(\rho(\mu_s - \mu_m))), \quad \mu_+''(y_0) = \rho c > 0, \quad \mu_+'''(y_0) = -\rho^2 c < 0.$$

In Fig. 5, we illustrate numerical results, obtained using AUTO, for (2.5) with the following parameters:

$$\mu_s = 1, \mu_m = 0.5, \rho = 4, c = 0.85,$$

such that $y_0 \approx 0.33$. In Fig. 5, we have also used the regularization function

$$\phi(s, \epsilon) = \frac{s}{\sqrt{s^2 + 1}}$$

so that $k = 2$ in (A2), and varied the small parameter ϵ . In Fig. 5(a), for example, a bifurcation diagram is shown using $\min y$ as a measure of the amplitude, with

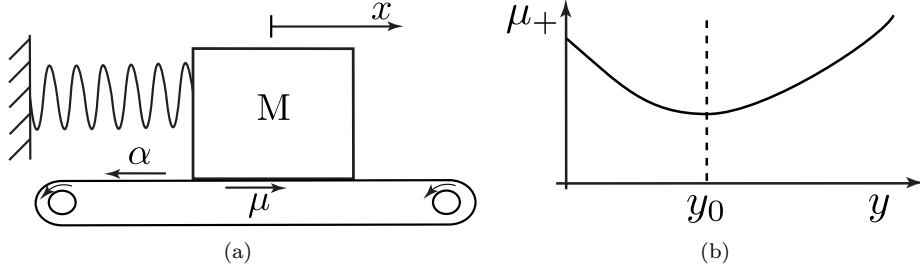


FIGURE 4. In (a): The mass-spring system on a moving belt. In (b): A Stribeck friction law with a minimum at $y = y_0$.

ϵ varying along the different branches, highlighted in different colours. The Hopf bifurcation occurs at $\alpha \approx y_0$ with $\min y$ decreasing from around that same value (not visible in the zoomed version of the diagram in (a)). However, along each branch, a saddle-node bifurcation is visible. In black dotted lines is the unperturbed bifurcation diagram for Z_+ . Numerically, we therefore see that the saddle-node bifurcation approaches the singular limit, as claimed in Theorem 1.4. See further details in the figure caption. In Fig. 5(d), we show the value of $\alpha_* - \alpha$ along the saddle-node bifurcation for varying values of ϵ using a loglog-scale. Here $\alpha_* \approx 0.4$ is the unperturbed value of the bifurcation, where the limit cycle of Z_+ grazes the discontinuity set. The slope of the curve is almost constant; using least square we obtain a slope ≈ 0.8024 which is in agreement with Theorem 1.4 for $k = 2$; notice $\epsilon^{2k/(2k+1)} = \epsilon^{4/5} = \epsilon^{0.8}$ for this value of k .

In Fig. 5(c), the nonhyperbolic periodic orbits are shown for different values of ϵ . The dotted black curve (barely visible, but it has the largest amplitude) shows the grazing limit cycle for Z_+ at $\alpha = \alpha_* \approx 0.4$. Finally, Fig. 5(d) shows two co-existing limit cycles for $\alpha = 0.38$ and $\epsilon = 5 \times 10^{-4}$ in red. For comparison, the bifurcating limit cycle at this ϵ -value and $\alpha = 0.398$ is shown using a red dotted line.

We discuss the friction oscillator problem further in Section 5.

3. PROOF OF THEOREM 1.1

To prove Theorem 1.1, we follow [22] and consider the slow time scale system

$$\begin{aligned} \dot{z} &= \epsilon Z(z, \phi(y\epsilon^{-1}, \epsilon), \epsilon, \alpha), \\ \dot{\epsilon} &= 0, \end{aligned}$$

and blowup $(y, \epsilon) = 0$ by

$$r \geq 0, (\bar{y}, \bar{\epsilon}) \in S^1 \mapsto (y, \epsilon) = r(\bar{y}, \bar{\epsilon}).$$

To describe this blowup we work in directional charts, following e.g. [23], obtained by setting $\bar{y} = 1$, $\bar{\epsilon} = 1$ and $\bar{y} = -1$, respectively. This produces the following local forms

$$r_1 \geq 0, \epsilon_1 \geq 0, \mapsto (y, \epsilon) = r_1(1, \epsilon_1), \quad (3.1)$$

$$r_2 \geq 0, y_2 \in \mathbb{R}, \mapsto (y, \epsilon) = r_2(y_2, 1), \quad (3.2)$$

$$r_3 \geq 0, \epsilon_3 \in \mathbb{R}, \mapsto (y, \epsilon) = r_3(-1, \epsilon_3), \quad (3.3)$$

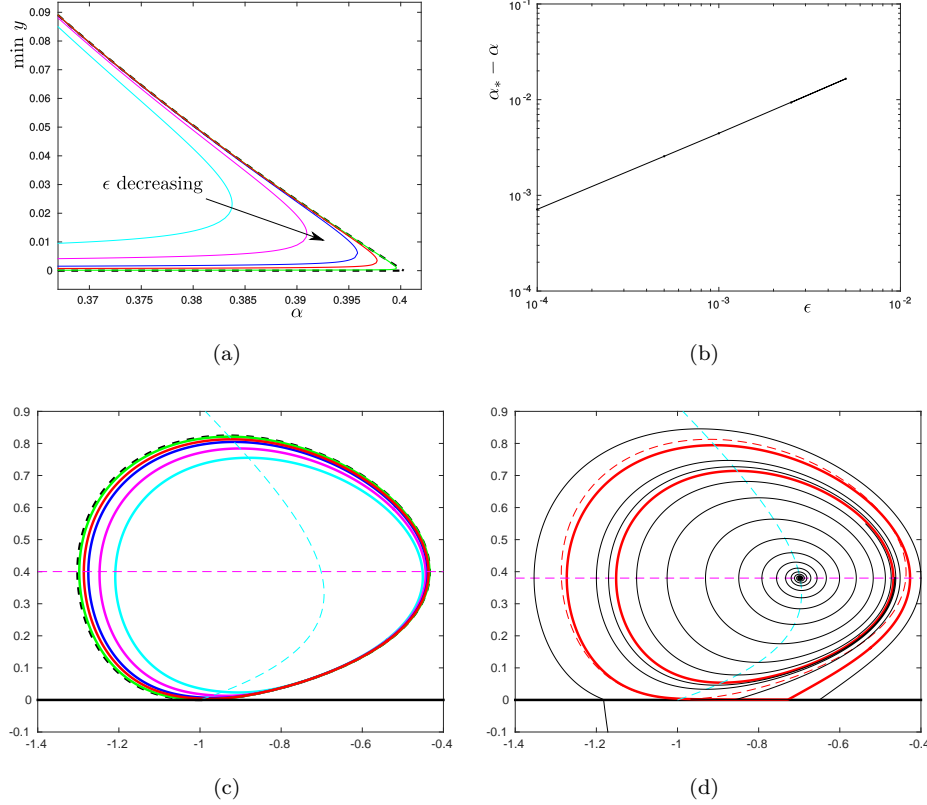


FIGURE 5. In (a): Bifurcation diagram of limit cycles using $\min y$ as a measure of the amplitude for varying values of ϵ : in cyan: $\epsilon = 5 \times 10^{-3}$, magenta: $\epsilon = 2.5 \times 10^{-3}$, blue: $\epsilon = 10^{-3}$, red: $\epsilon = 5 \times 10^{-4}$, and finally in green: $\epsilon = 10^{-4}$. In (b): $\alpha_* - \alpha$ along the saddle-node bifurcation for varying values of ϵ . The slope is nearly constant ≈ 0.8024 , in good agreement with the theoretical value of $4/5$ obtained from Theorem 1.4 with $k = 2$. In (c): the saddle-node limit cycles. The dotted magenta and cyan curves are nullclines for Z_+ at the unperturbed bifurcation parameter $\alpha = 0.4$. The colours are identical to (a). In (d), for $\epsilon = 5 \times 10^{-3}$, two limit cycles are shown for $\alpha = 0.38$. The inner most is unstable while the other one, having a segment near the sliding region, is stable. The black curves are transients while the dotted magenta and cyan curves are nullclines as in (b). For comparison, the saddle-node periodic orbit (red and dotted) is shown for the same ϵ -value.

respectively. We will enumerate these three charts as $(\bar{y} = 1)_1$, $(\bar{\epsilon} = 1)_2$ and $(\bar{y} = -1)_3$, respectively, giving reference to how the charts are obtained and the subscripts used. We prove part (a) of the theorem by working in these three charts. The result is standard and can be found in different formulations, also for more

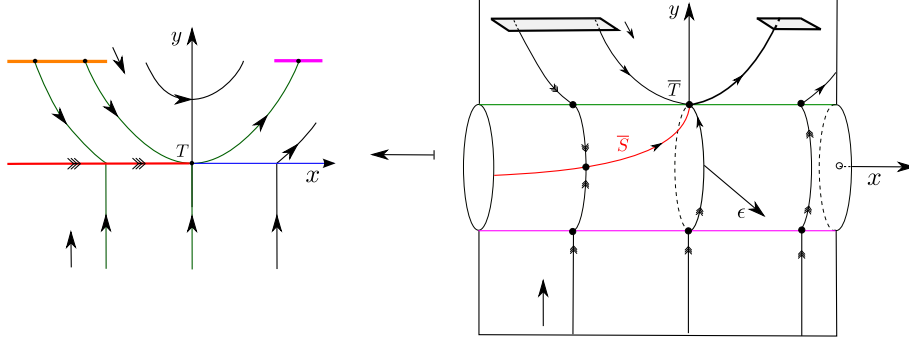


FIGURE 6. Illustration of the cylindrical blowup of the visible fold.

general systems. See [26, 22] for example. We therefore delay the details to Appendix A and instead just summarise the findings, see also Fig. 6: Using $(\bar{\epsilon} = 1)_2$ we find a critical manifold \bar{S} on the cylinder as a graph over Σ_{sl} . It is noncompact and using $(\bar{y} = 1)_1$ we find that it ends on the edge $\bar{y} = 1$ in a nonhyperbolic point $\bar{T}: x = 0, (\bar{y}, \bar{\epsilon}) = (1, 0)$, which is the imprint of the tangency T on the regularized, blown-up system. Away from $x = 0$ the edge $\bar{y} = 1$ is hyperbolic, whereas $\bar{y} = -1$ is hyperbolic for all x . The latter property follows from working in $(\bar{y} = -1)_3$. Next, by working in $(\bar{\epsilon} = 1)_2$, we obtain the invariant manifold S_ϵ using Fenichel's theory upon restricting \bar{S} to the compact set $x \in J$. The invariant foliation is also a consequence of Fenichel's theory. However, Fenichel's foliation is only local to \bar{S} on the cylinder. To extend it beyond into $y \neq 0$ uniformly in ϵ we work near the hyperbolic lines $(\bar{y}, \bar{\epsilon}) = (\pm 1, 0)$, $x < 0$ in the charts $(\bar{y} = \pm 1)_{1,3}$, respectively. See Appendix A.

To prove the remaining claims of the theorem, we work in chart $(\bar{y} = 1)_1$ with the coordinates (r_1, x, ϵ_1) and the local blowup (3.1). This gives the following equations:

$$\begin{aligned}\dot{r} &= rF(r, x, \epsilon), \\ \dot{x} &= r(1 - \epsilon^k \phi_1(r, \epsilon))(1 + f(x, r)), \\ \dot{\epsilon} &= -\epsilon F(r, x, \epsilon),\end{aligned}$$

after division of the right hand side by the common factor ϵ_1 , where

$$F(r, x, \epsilon) = (1 - \epsilon^k \phi_1(r, \epsilon))(2x + rg(x, r)) + \epsilon^k \phi_1(r, \epsilon),$$

having here also dropped the subscripts on r_1 and ϵ_1 . To obtain these expressions we have used (A2) and set $k_+ = k$, for simplicity. Clearly, $(r, x, \epsilon) = (0, 0, 0)$ is fully nonhyperbolic. Therefore we blowup this point by a k -dependent blowup transformation:

$$\rho \geq 0, (\bar{r}, \bar{x}, \bar{\epsilon}) \in S^2 \mapsto \begin{cases} r = \rho^{2k} \bar{r}, \\ x = \rho^k \bar{x}, \\ \epsilon = \rho \bar{\epsilon}. \end{cases} \quad (3.4)$$

The exponents (or weights) $2k$, k , and 1 on ρ in these expressions are so that the vector-field has ρ^k as a common factor. We therefore desingularize by dividing out this common factor and achieve improved hyperbolicity properties.

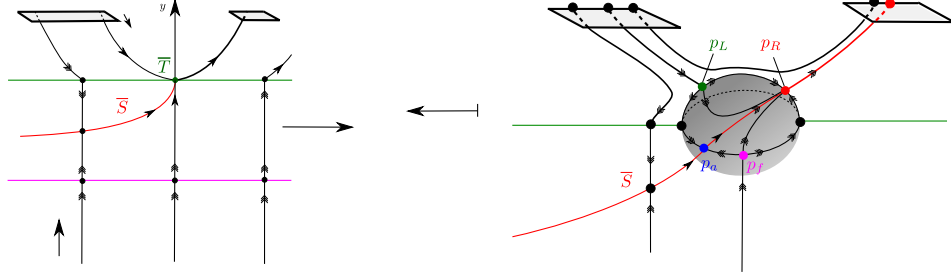


FIGURE 7. Illustration of the subsequent blowup (3.4) of the non-hyperbolic point $(r_1, x_1, \epsilon_1) = (0, 0, 0)$ in the chart $(\bar{y} = 1)_1$. The weights in (3.4) are so that the critical manifold and the non-hyperbolic fiber gets separated into two points p_a and p_f on the sphere. By desingularization, these points have improved hyperbolicity properties. Similarly, the blowup also separates the quadratic tangency within $\epsilon = 0$ into two points p_L and p_R on the sphere, which also have improved hyperbolicity properties after desingularization. See Lemma 3.2 and Lemma 3.7.

Remark 3.1. Notice that the weights in the expressions for x and ϵ in (3.4) are so that on the cylinder $\{r = 0\}$, the k th-order tangency between the critical manifold, of the form $x = \epsilon_1^k m(\epsilon_1)$, and the nonhyperbolic critical fiber, at $x = \epsilon_1 = 0$, gets geometrically separated on the blowup sphere. Similarly, the weights on x and $y = r$ are so that the quadratic tangency within $\{\epsilon = 0\}$, due to the visible fold, also gets separated.

We will use three local charts, obtained by setting $\bar{r} = 1$, $\bar{\epsilon} = 1$ and $\bar{x} = -1$, to describe this blowup:

$$(\bar{r} = 1)_1 : \rho_1 \geq 0, x_1 \in \mathbb{R}, \epsilon_1 \geq 0 \mapsto \begin{cases} r &= \rho_1^{2k}, \\ x &= \rho_1^k x_1, \\ \epsilon &= \rho_1 \epsilon_1, \end{cases} \quad (3.5)$$

$$(\bar{\epsilon} = 1)_2 : \rho_2 \geq 0, r_2 \geq 0, x_2 \in \mathbb{R} \mapsto \begin{cases} r &= \rho_2^{2k} r_2, \\ x &= \rho_2^k x_2, \\ \epsilon &= \rho_2, \end{cases} \quad (3.6)$$

$$(\bar{x} = -1)_3 : \rho_3 \geq 0, r_3 \geq 0, \epsilon_3 \geq 0 \mapsto \begin{cases} r &= \rho_3^{2k} r_3, \\ x &= -\rho_3^k, \\ \epsilon &= \rho_3, \end{cases} \quad (3.7)$$

As indicated, these charts are enumerated as $(\bar{r} = 1)_1$, $(\bar{\epsilon} = 1)_2$ and $(\bar{x} = -1)_3$, respectively. We illustrate the blowup in Fig. 7, representing now, on the left, the cylinder in Fig. 6 as a strip (looking from the side). We consider each of the charts in the following.

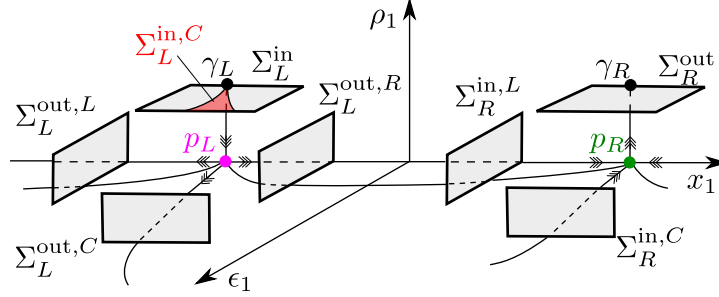


FIGURE 8. Illustration of the dynamics in chart $(\bar{r} = 1)_1$, see (3.5). p_L and p_R are hyperbolic and we use partial, smooth linearizations, see Lemma 3.3 and Lemma 3.4, near this points to describe the local transition maps between the various sections shown.

3.1. **Chart $(r = 1)_1$.** In this chart, we obtain the following equations:

$$\begin{aligned} \dot{\rho}_1 &= \frac{1}{2k} \rho_1 F_1(\rho_1, x_1, \epsilon_1), \\ \dot{x}_1 &= (1 - \rho_1^k \epsilon_1^k \phi_1(\rho_1^{2k}, \rho_1 \epsilon_1))(1 + \rho_1^k f_1(\rho_1^k, x_1)) - \frac{1}{2} F_1(\rho_1, x_1, \epsilon_1) x_1, \\ \dot{\epsilon}_1 &= -\frac{2k+1}{2k} F_1(\rho_1, x_1, \epsilon_1), \end{aligned} \quad (3.8)$$

where

$$F_1(\rho_1, x_1, \epsilon_1) = (1 - \rho_1^k \epsilon_1^k \phi_1(\rho_1^{2k}, \rho_1 \epsilon_1))(2x_1 + \rho_1^k g_1(\rho_1^k, x_1)) + \epsilon_1^k \phi_1(\rho_1^{2k}, \rho_1 \epsilon_1),$$

and

$$f_1(\rho_1^k, x_1) = \rho_1^{-k} f(\rho_1^k x_1, \rho_1^{2k}), \quad g_1(\rho_1^k, x_1) = g(\rho_1^k x_1, \rho_1^{2k}).$$

Notice that f_1 is well-defined and smooth since $f(0, 0) = 0$. Also, $\rho_1 = \epsilon_1 = 0$ is invariant. Along this axis we have

$$\dot{x}_1 = 1 - x_1^2.$$

Therefore $x_1 = \mp 1$ are equilibria of this reduced system, $x_1 = -1$ being hyperbolic and unstable, $x_1 = 1$ being hyperbolic and stable.

Lemma 3.2. *The points $p_L, p_R : (\rho_1, x_1, \epsilon_1) = (0, \mp 1, 0)$, respectively, are hyperbolic. In particular, the eigenvalues of p_L and p_R are as follows:*

$$\begin{aligned} \text{for } p_L : \lambda_1 &= -\frac{1}{k}, \lambda_2 = 2, \lambda_3 = 2 + \frac{1}{k}, \\ \text{for } p_R : \lambda_1 &= -2 - \frac{1}{k}, \lambda_2 = -2, \lambda_3 = \frac{1}{k}. \end{aligned}$$

Moreover, the 2-dimensional $W_{loc}^u(p_L)$ is a neighborhood of $x_1 = -1$, $\epsilon_1 = 0$ within $\rho_1 = 0$ whereas the 1-dimensional $W^s(p_L)$ is tangent to the vector $(1, 0, 0)$. On the other hand, the 2-dimensional $W_{loc}^s(p_R)$ is a full neighborhood of $x_1 = 1$, $\epsilon_1 = 0$ within $\rho_1 = 0$ whereas the 1-dimensional $W^u(p_R)$ is tangent to the vector $(1, 0, 0)$.

Proof. Calculation. □

See Fig. 8 for illustration, compare also with the sphere on the right in Fig. 7. Notice that there are strong resonances at p_L/R :

$$\lambda_2 - \lambda_1 - \lambda_3 = 0,$$

and hence we cannot (directly, at least) perform a C^1 -linearization. However, near p_L and p_R we have $F_1 \approx \mp 2$, respectively, and we can therefore divide the right hand side of the equations by $-\frac{1}{2}F_1$ and $\frac{1}{2}F_1$, respectively, in a neighborhood of these points. Near p_L , for example, this produces

$$\begin{aligned} \dot{\rho}_1 &= -\frac{1}{k}\rho_1, \\ \dot{x}_1 &= x_1 - \frac{2(1 + \rho_1^k f_1(\rho_1^k, x_1))}{2x_1 + \rho_1^k g_1(\rho_1^k, x_1)} + \epsilon_1^k G_1(\rho_1, x_1, \epsilon_1), \\ \dot{\epsilon}_1 &= \frac{2k+1}{k}\epsilon_1, \end{aligned} \tag{3.9}$$

for some smooth G_1 . Now, we consider $\epsilon_1 = 0$:

$$\begin{aligned} \dot{\rho}_1 &= -\frac{1}{k}\rho_1, \\ \dot{x}_1 &= x_1 - \frac{2(1 + \rho_1^k f_1(\rho_1^k, x_1))}{2x_1 + \rho_1^k g_1(\rho_1^k, x_1)}. \end{aligned}$$

Lemma 3.3. *There exists a near-identity diffeomorphism*

$$(\tilde{\rho}_1, \tilde{x}_1) \mapsto \begin{cases} \rho_1 &= \tilde{\rho}_1 Q_1(\tilde{\rho}_1^k, \tilde{x}_1), \\ x_1 &= \tilde{x}_1 P_1(\tilde{\rho}_1^k, \tilde{x}_1), \end{cases} \tag{3.10}$$

where

$$Q_1(\tilde{\rho}_1^k, \tilde{x}_1), P_1(\tilde{\rho}_1^k, \tilde{x}_1) = 1 + \mathcal{O}(\tilde{\rho}_1^k), \tag{3.11}$$

defined for $\tilde{x}_1 \in I$, I a fixed open large interval, and $\tilde{\rho}_1 \in [0, \xi]$. Furthermore, there exists a smooth and a positive function T defined on the same set satisfying $T(0, \tilde{x}_1) = 1$ for all \tilde{x}_1 such that

$$\begin{aligned} \dot{\tilde{\rho}}_1 &= -\frac{1}{k}\tilde{\rho}_1 T(\tilde{\rho}_1, \tilde{x}_1), \\ \dot{\tilde{x}}_1 &= \left(\tilde{x}_1 - \frac{1}{\tilde{x}_1}\right) T(\tilde{\rho}_1, \tilde{x}_1). \end{aligned}$$

in a neighborhood of $(\tilde{\rho}_1, \tilde{x}_1) = (0, -1)$.

Proof. By the flow-box theorem there exists a smooth, local diffeomorphism conjugating

$$\begin{aligned} \dot{x} &= 1 + f(x, y), \\ \dot{y} &= 2x + yg(x, y), \end{aligned}$$

with

$$\begin{aligned} \dot{\tilde{x}} &= 1, \\ \dot{\tilde{y}} &= 2\tilde{x}, \end{aligned}$$

of the form

$$(\tilde{x}, \tilde{y}) \mapsto \begin{cases} x &= \tilde{x}Q(\tilde{x}, \tilde{y}), \\ y &= \tilde{y} + P(\tilde{x}, \tilde{y}), \end{cases}$$

where $Q(0,0) = 1$ and P is quadratic. Notice that the transformation fixes the first axis. Furthermore, calculations also show that $P(x,y) - g(0,0)xy = \mathcal{O}(3)$. Now, we insert $\tilde{y} = \tilde{\rho}_1^{2k}$, $\tilde{x} = \tilde{\rho}_1^k \tilde{x}_1$ and $y = \rho_1^{2k}$ and $x = \rho_1^k x_1$. This produces (3.10). A straightforward calculation verifies the property in the lemma. \square

Next, we define $\tilde{\epsilon}_1$ by

$$\epsilon_1 = \tilde{\epsilon}_1 Q_1(\tilde{\rho}_1^k, \tilde{x}_1)^{-2k-1},$$

which is invertible locally by (3.11) and the implicit function theorem. Recall that $\rho_1^{2k+1} \epsilon_1 = \epsilon$ const. Therefore by construction $\tilde{\rho}_1^{2k+1} \tilde{\epsilon}_1 = \epsilon$ also in the new coordinates. In total:

Lemma 3.4. *The diffeomorphism*

$$(\tilde{\rho}_1, \tilde{x}_1, \tilde{\epsilon}_1) \mapsto \begin{cases} \rho_1 &= \tilde{\rho}_1 Q_1(\tilde{\rho}_1^k, \tilde{x}_1), \\ x_1 &= \tilde{x}_1 P_1(\tilde{\rho}_1^k, \tilde{x}_1), \\ \epsilon_1 &= \tilde{\epsilon}_1 Q_1(\tilde{\rho}_1^k, \tilde{x}_1)^{-2k-1}, \end{cases}$$

transforms (3.9) into

$$\begin{aligned} \dot{\tilde{\rho}}_1 &= -\frac{1}{k} \tilde{\rho}_1 T(\tilde{\rho}_1, \tilde{x}_1), \\ \dot{\tilde{x}}_1 &= \left(\tilde{x}_1 - \frac{1}{\tilde{x}_1} \right) T(\tilde{\rho}_1, \tilde{x}_1) + \tilde{\epsilon}_1^k \tilde{G}_1(\tilde{\rho}_1, \tilde{x}_1, \tilde{\epsilon}_1), \\ \dot{\tilde{\epsilon}}_1 &= \frac{2k+1}{k} \tilde{\epsilon}_1 T(\tilde{\rho}_1, \tilde{x}_1). \end{aligned}$$

We now drop the tildes and transform time by dividing through by T . This gives

$$\begin{aligned} \dot{\rho}_1 &= -\frac{1}{k} \rho_1, \\ \dot{x}_1 &= x_1 - \frac{1}{x_1} + \epsilon_1^k G_1(\rho_1, x_1, \epsilon_1), \\ \dot{\epsilon}_1 &= \frac{2k+1}{k} \epsilon_1. \end{aligned}$$

Next, for the $\rho_1 = 0$ sub-system the linearization about $x_1 = -1$, $\epsilon_1 = 0$ produces eigenvalues λ_2 and λ_3 which are nonresonant. Therefore there exists a smooth local diffeomorphism that linearizes the $\rho_1 = 0$ -system. Applying this transformation to the full system produces

$$\begin{aligned} \dot{\rho}_1 &= -\frac{1}{k} \rho_1, \\ \dot{x}_1 &= 2x_1 + \epsilon_1^k G_1(\rho_1, x_1, \epsilon_1), \\ \dot{\epsilon}_1 &= \frac{2k+1}{k} \epsilon_1, \end{aligned}$$

for some new smooth $G_1 = \mathcal{O}(\rho_1 \epsilon_1 + \rho_1^k)$, using the same symbols for simplicity. We illustrate the local dynamics in Fig. 8. Notice that Σ_L , in the new coordinates, has become

$$\Sigma_L^{\text{in}} = \{(\rho_1, x_1, \epsilon_1) | \rho_1 = \delta > 0, x_1 \in [-\beta_1, \beta_1], \epsilon_1 \in [0, \beta_2]\},$$

containing γ_L as $\rho_1 = \delta, x_1 = 0, \epsilon_1 = 0$ in these coordinates.

Lemma 3.5. *Fix $c > 0$ sufficiently small and consider the wedge*

$$\Sigma_L^{in,C} = \Sigma_L \cap \{|x_1| \leq c^{-1} \epsilon_1^{2k/(2k+1)}\}, \quad (3.12)$$

consisting of all points in Σ_L^{in} with $|x_1| \leq c^{-1} \epsilon_1^{2k/(2k+1)}$, and the section

$$\Sigma_L^{out,C} = \{(\rho_1, x_1, \epsilon_1) | \rho_1 \in [0, \beta_3], x_1 \in [-\beta_4, \beta_4], \epsilon_1 = \nu\}.$$

Then there exists δ, ν and $\beta_i, i = 1, \dots, 4$ such that the transition map $P_L^C : \Sigma_L^{in,C} \rightarrow \Sigma_L^{out,C}$ obtained by the forward flow is well-defined and of the following form

$$P_L^C(\delta, x_1, \epsilon_1) = \begin{pmatrix} (\epsilon_1 \nu^{-1})^{1/(2k+1)} \delta \\ X_L^C(x_1, \epsilon_1) \\ \nu \end{pmatrix}$$

where $X_L^C(\cdot, \epsilon_1)$ is C^2 $\mathcal{O}(\epsilon_1^{1/(2k+1)})$ -close to the linear map $x_1 \mapsto (\epsilon_1 \nu^{-1})^{-2k/(2k+1)} x_1$:

$$X_L^C(x_1, \epsilon_1) = (\epsilon_1 \nu^{-1})^{-2k/(2k+1)} x_1 + \mathcal{O}(\epsilon_1^{1/(2k+1)}).$$

Proof. We integrate the ρ_1 and ϵ_1 equation and insert this into the x_1 -equation. We then write $x_1 = e^{2t}u$ and estimate u through direct integration. Returning to x_1 gives the desired result. The derivatives of X_L^C with respect to x_1 can be handled in the exact same way by looking at the variational equations. The estimates on u do not change by this differentiation. \square

Returning to (3.8), we can perform the exact same analysis near p_R . In other words: Near p_R there exists a transformation of the form (3.10), see Lemma 3.3, for some new Q_1 and P_1 , that brings the system into the following form, after dropping the tildes and transformation of time:

$$\begin{aligned} \dot{\rho}_1 &= \frac{1}{k} \rho_1, \\ \dot{x}_1 &= -x_1 + \frac{1}{x_1} + \epsilon_1^k \tilde{G}_1(\rho_1, x_1, \epsilon_1), \\ \dot{\epsilon}_1 &= -\frac{2k+1}{k} \epsilon_1. \end{aligned}$$

Here we again abuse notation slightly and reuse the symbol \tilde{G}_1 for a new smooth function. Finally upon linearization of the $\rho_1 = 0$ subsystem, through a near-identity, ϵ_1 -dependent transformation of x_1 , we obtain the system

$$\begin{aligned} \dot{\rho}_1 &= \frac{1}{k} \rho_1, \\ \dot{x}_1 &= -2x_1 + \epsilon_1^k G_1(\rho_1, x_1, \epsilon_1), \\ \dot{\epsilon}_1 &= -\frac{2k+1}{k} \epsilon_1, \end{aligned} \quad (3.13)$$

using the same symbol for the new x_1 . Here $G_1 = \mathcal{O}(\epsilon_1 \rho_1 + \rho_1^k)$.

In these coordinates, Σ_R has become

$$\Sigma_R^{out} = \{(\rho_1, x_1, \epsilon_1) | \rho_1 = \delta > 0, x_1 \in [-\beta_1, \beta_1], \epsilon_1 \in [0, \beta_2]\}$$

containing $\gamma_L : \rho_1 = 0, x_1 = 0, \epsilon_1 = 0$.

Lemma 3.6. *Consider the section*

$$\Sigma_R^{in,C} = \{(\rho_1, x_1, \epsilon_1) | \rho_1 \in [0, \beta_3], x_1 \in [-\beta_4, \beta_4], \epsilon_1 = \nu\}.$$

Then there exists δ , ν and β_i , $i = 1, \dots, 4$ such that the transition map $P_R^C : \Sigma_R^{in,C} \rightarrow \Sigma_R^{out,C}$ obtained by the forward flow is well-defined and of the following form

$$P_R^C(\rho_1, x_1, \nu) = \begin{pmatrix} \delta \\ X_R^C(x_1, \rho_1) \\ (\rho_1 \delta^{-1})^{2k+1} \nu \end{pmatrix}$$

where $X_R^C(\cdot, \epsilon_1)$ is C^2 $\mathcal{O}(\rho_1^{2k+1})$ -close to the linear map $x_1 \mapsto (\epsilon_1 \nu^{-1})^{2k/(2k+1)} x_1$:

$$X_R^C(x_1, \epsilon_1) = (\rho_1 \delta^{-1})^{2k} x_1 + \mathcal{O}(\rho_1^{2k+1}). \quad (3.14)$$

Proof. Identical to the proof of Lemma 3.5. Details are therefore left out. \square

3.2. Chart $(\epsilon = 1)_2$. In this chart, we obtain the following equations

$$\begin{aligned} \dot{\rho}_2 &= -\rho_2 F_2(\rho_2, r_2, x_2), \\ \dot{r}_2 &= (2k+1)r_2 F_2(\rho_2, r_2, x_2), \\ \dot{x}_2 &= r_2 (1 - \rho_2^k \phi_1(\rho_2^{2k} r_2, \rho_2)) (1 + \rho_2^k f_2(\rho_2, r_2, x_2)) + k x_2 F_2(\rho_2, r_2, x_2), \end{aligned}$$

where

$$F_2(\rho_2, r_2, x_2) = (1 - \rho_2^k \phi_1(\rho_2^{2k} r_2, \rho_2))(2x_2 + \rho_2^k r_2 g_2(\rho_2^k, r_2, x_2)) + \phi_1(\rho_2^{2k} r_2, \rho_2),$$

and

$$f_2(\rho_2^k, r_2, x_2) = \rho_2^{-k} f(\rho_2^k x_2, \rho_2^{2k} r_2), \quad g_2(\rho_2^k, r_2, x_2) = g(\rho_2^k x_2, \rho_2^{2k} r_2).$$

Along the invariant set $\rho_2 = r_2 = 0$, we have

$$\dot{x}_2 = k x_2 (2x_2 + \phi_1(0, 0)),$$

so that $x_2 = 0$ and $x_2 = -\frac{1}{2}\phi_1(0, 0)$ are equilibria, the former being unstable while the latter is stable. Linearization of the full system about these equilibria gives

Lemma 3.7. *We have*

- *The point $p_a : (\rho_2, r_2, x_2) = (0, 0, -\frac{1}{2}\phi_1(0, 0))$ is partially hyperbolic, the linearization having only one single non-zero eigenvalue $\lambda = -k\phi_1(0, 0) < 0$. As a consequence there exists a center manifold M_1 of p_a which contains S_1 within $r_2 = 0$ as a manifold of equilibria and a unique center manifold within $\rho_2 = 0$, along which r_2 is increasing, which is tangent to the eigenvector $(0, k\phi_1, 1)^T$. The equilibrium p_a is therefore a nonhyperbolic saddle.*
- *The point $p_f : (\rho_2, r_2, x_2) = (0, 0, 0)$ is fully hyperbolic, the linearization having two positive eigenvalues and one negative. The stable manifold is $r_2 = x_2 = 0$, $\rho_2 \geq 0$ whereas W_{loc}^u is a neighborhood of $(r_2, x_2) = (0, 0)$ within $\rho_2 = 0$.*

Proof. Calculations. \square

3.3. Proof of Theorem 1.1(b) and (c). In chart $(\bar{\epsilon} = 1)_2$, the set defined by the following equation

$$\rho_2^{2k+1} r_2^{2k} = \epsilon, \quad (3.15)$$

where ϵ is the original small parameter, is invariant. This follows from (3.6) and (3.1). Therefore if we fix $\epsilon > 0$ sufficiently small and restrict to the set defined by (3.15), the local center manifold M_1 in Lemma 3.7 provides an extension of the invariant manifold S_ϵ up to $r_2 = v$, v a small const, in the usual way; see e.g. [23]. At $r_2 = v$ we have

$$\rho_2 = (\epsilon v^{-2k})^{1/(2k+1)},$$

by (3.15), and hence

$$y = \rho_2^{2k} r_2 = (\epsilon v^{-2k})^{2k/(2k+1)} v.$$

In fact, following the analysis of the standard, slow-fast, planar, regular fold point in [23] we obtain a similar result to [23, Proposition 2.8] for the local transition map from $\rho_2 = \nu$ to $r_2 = v$ near p_a that is exponentially contracting like $e^{-cr_2^{-1}}$ with $c > 0$.

Next, since r_2 is increasing on M_1 , we may track the slow manifold across the sphere, using regular perturbation, Poincaré-Bendixson and the analysis in $(\bar{r} = 1)_1$ in the previous subsection, up close to p_R . We then use Lemma 3.6 and the mapping P_R^C to describe the passage near p_R . Recall that p_R is a stable node on the sphere, attracting every point on the quarter sphere $\bar{\epsilon} \geq 0$, $\bar{r} \geq 0$, except for certain subsets of the invariant half-circles $\bar{r} = 0$ and $\bar{\epsilon} = 0$. See Fig. 7. By the expression in (3.14), and the following conservation

$$\rho_1 = (\epsilon \delta)^{1/(2k+1)}, \quad (3.16)$$

in chart $(\bar{r} = 1)_1$ at $\epsilon_1 = \delta$ on $\Sigma_R^{\text{in},C}$, obtained by combining (3.6) and (3.1), we reach the result on the slow manifold in Theorem 1.1(b). Also, combining the exponential contraction near p_a in chart $(\bar{\epsilon} = 1)_2$ with the algebraic contraction in Lemma 3.6, we obtain the contraction of the local map $Q|_K$ as detailed in Theorem 1.1(c).

3.4. Proof of Theorem 1.1(d). For the proof Theorem 1.1(d), we focus on the estimate (ii). The estimates (i) and (iii) are simpler and we will only discuss these at the end of this section. The idea for (ii) is to first work in $(\bar{r} = 1)_1$ near p_L . The domain for x in (ii) allow us to apply P_L^C , possibly after adjusting the relevant constants. This brings us up to $\epsilon_1 = \nu$ and $x_1 + 1 \in [-\beta_4, \beta_4]$. From here, working in chart $(\bar{\epsilon} = 1)_2$, we can guide the flow using regular perturbation theory up to p_R , where we can apply (again after possibly adjusting relevant constants) P_R^C .

Now, P_L^C is expanding by $c_L \epsilon^{-2k/(2k+1)}$ to leading order, for some constant $c_L > 0$, in the x_1 -direction. But, upon adjusting the domains appropriately, P_R^C is contracting by the exact same factor, see Lemma 3.6 and (3.16). As a consequence, for any $c > 0$ there exist constants such that $P_R^C \circ P_L^C$ is c -close in C^2 to the identity map. Therefore, when writing Q as a composition, in the chart $(\bar{\rho} = 1)_1$, of P_L^C , followed by a mapping P_C from $\Sigma_L^{\text{out},C}$ to $\Sigma_R^{\text{in},C}$, and lastly P_R^C , the contractive properties of Q are therefore essentially given by P_C only.

To study P_C we consider first the $\rho_1 = 0$ -subsystem in chart $(\bar{\rho} = 1)_1$:

$$\begin{aligned}\dot{x}_1 &= 1 - \frac{1}{2} \{2x_1 + \epsilon_1^k \phi_1\} x_1, \\ \dot{\epsilon}_1 &= -\frac{2k+1}{2k} \{2x_1 + \epsilon_1^k \phi_1\} \epsilon_1.\end{aligned}\tag{3.17}$$

Here and in the following, we will for simplicity write $\phi_1(0, 0)$ as ϕ_1 . We now use the fact that the curly bracket in (3.17) appears in both equations to come up with better coordinates:

Lemma 3.8. *The diffeomorphism defined by*

$$(\epsilon_1, x_1) \mapsto \begin{cases} u &= (\phi_1 \epsilon_1^k)^{-1/(2k+1)} x_1, \\ v &= (\phi_1 \epsilon_1^k)^{-2/(2k+1)}, \end{cases}$$

for $\epsilon_1 > 0$, brings (3.17) into the following system

$$\begin{aligned}\dot{u} &= v^{1/2}, \\ \dot{v} &= v^{1/2} (2u + v^{-k}).\end{aligned}\tag{3.18}$$

Proof. Simple calculation. \square

To study (3.18) we multiply the right hand side by $v^{-1/2}$:

$$\begin{aligned}\dot{u} &= 1, \\ \dot{v} &= 2u + v^{-k},\end{aligned}\tag{3.19}$$

Remark 3.9. *The equation (3.19), written as a first order system, is known as a Chini equation, see e.g. [28]. To the best of the author's knowledge, no solution by quadrature is known to exist. As a result, our analysis of this system is fairly indirect.*

In the (u, v) -coordinates, $\Sigma_L^{\text{out}, C}$ and $\Sigma_R^{\text{in}, C}$ both become subsets of $v = \nu^{-2k/(2k+1)}$, with $u < 0$ and $u > 0$ respectively. For simplicity, we drop the superscripts on Σ_L and Σ_R in the following. Given the form of (3.19), we can therefore write the mapping P_C for $\rho_1 = 0$ as

$$u \mapsto P_C(u),$$

abusing notation slightly, where

$$P_C(u) = T(u) + u,\tag{3.20}$$

$T(u)$ being the time of flight, see Fig. 9 and (3.22) below.

Lemma 3.10. *The following holds*

$$P'_C(u) \in (-1, 0), \quad P''_C(u) < 0,\tag{3.21}$$

for all $(u, \nu^{-2k/(2k+1)}) \in \Sigma_L$.

Proof. We will in the following estimate $T'(u)$ and $T''(u)$, consecutively. Let $c = \nu^{-2k/(2k+1)}$ and write the solution of (3.19) with initial conditions $(u_0, c) \in \Sigma_L$ as $(u(t, u_0), v(t, u_0))$. Then $T(u_0) > 0$ is the least positive solution satisfying

$$v(T(u_0), u_0) = c.\tag{3.22}$$

Differentiating (3.22) gives

$$T'(u_0) = -\frac{v'_u(T(u_0), u_0)}{v'_t(T(u_0), u_0)}. \quad (3.23)$$

Notice that if

$$v'_u(T(u_0), u_0) < 2v'_t(T(u_0), u_0), \quad (3.24)$$

then, by (3.23),

$$T'(u_0) > -2. \quad (3.25)$$

Since $P'_C(u) < 0$ is trivial, this inequality implies the first claim in (3.21) by differentiating (3.20). To show (3.24) let $v_1(t) = v'_u(t, u_0)$ so that $v_1(0) = 0$ and

$$\dot{v}_1 = 2 - kv^{-k-1}v_1. \quad (3.26)$$

Clearly, $v_1(t) > 0$ for all $t > 0$. Now, $\dot{v}(t, u_0) = v'_t(t, u_0)$ also satisfies the equation (3.26), but with the initial condition $\dot{v}(0, u_0) = 2u_0 + c^{-k} < 0$. In light of (3.24), we therefore write v_1 as

$$v_1 = 2\dot{v} - w. \quad (3.27)$$

A simple calculations, shows that $w = w(t, u_0)$ also satisfies (3.26):

$$\dot{w} = 2 - kv^{-k-1}w, \quad (3.28)$$

but now $w(0, u_0) = 2\dot{v}(0, u_0) < 0$. We will now show that for all u_0

$$0 < w(T(u_0), u_0). \quad (3.29)$$

Adding $v_1 = 2\dot{v}(T(u_0), u_0) - w(T(u_0), u_0)$ to both sides of this equation, using (3.27), produces (3.24) and therefore (3.25) as desired.

For (3.29), notice by (3.28) that $\dot{w} \geq 2$ for all $w \leq 0$. Hence there exists a unique $t_*(u_0)$ such that

$$w(t_*(u_0), u_0) = 0. \quad (3.30)$$

Notice that $t_*(u_0)$ is a smooth function of u_0 by the implicit function theorem. Next, for values of $u_0 < -c^{-k}/2$, sufficiently close to $-c^{-k}/2$ (the value of u when the v -nullcline intersects $v = c$), a simple calculation shows that

$$T'(u_0) = -2 - \frac{2}{3}kc^{-k-1}(c^{-k} + 2u_0) + \mathcal{O}\left((c^{-k}/2 + u_0)^2\right) > -2,$$

and $t_*(u_0) < T(u_0)$. Hence, for these values of u_0 , it follows that (3.29), and therefore also (3.25), holds.

Suppose that upon decreasing u_0 we find a first u_* such that $T(u_*) = t_*(u_*)$. Notice then by (3.23) and (3.27) that $T'(u_*) = -2$, and

$$t'_*(u_*) \leq -2, \quad (3.31)$$

since $t_*(u_0) < T(u_0)$ for all $u_0 \in (u_*, -c^{-k})$, by assumption. Then, by differentiating (3.30),

$$t'_*(u_*) = -\frac{w_1(t_*(u_*), u_*)}{\dot{w}(t_*(u_*), u_*)} = -\frac{w_1(t_*(u_*), u_*)}{2}. \quad (3.32)$$

where w_1 satisfies the equation

$$\dot{w}_1 = -kv^{-k-1}w_1 + k(k+1)v^{-k-2}wv_1, \quad (3.33)$$

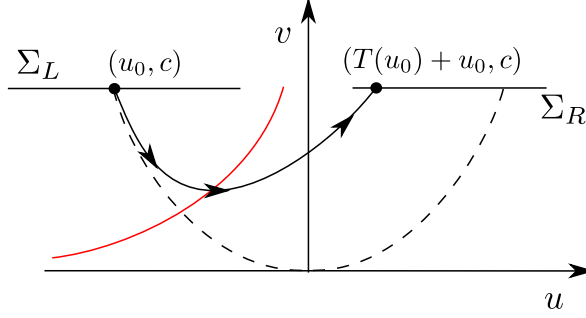


FIGURE 9. Dynamics within the (u, v) -plane. We describe the transition map from Σ_L and Σ_R using a simple analysis of the variational equations, which in the (u, v) -variables, take a simple form.

with $w_1(0) = 4$. In (3.32), we have also used that $\dot{w} = 2$ at $t = t_*$ where $w = 0$. Since $w(t, u_*) < 0$ for all $t \in [0, t_*(u_*)]$, and $v_1(t, u_*) > 0$ for all t , we have by (3.33) that $w_1(t_*(u_*), u_*) < 4$. But then by (3.32)

$$t'_*(u_*) > -2.$$

However, this contradicts (3.31) and hence no u_* exists. Consequently, $T(u_0) > t_*(u_0)$ for all $u_0 < -c^{-k}/2$ and therefore (3.25) holds.

For the subsequent claim in (3.21), we obtain the following expression for $T''(u_0)$

$$T''(u_0) = -\frac{1}{v'_t(T(u_0), u_0)} (2T'(u_0)P'_C(u_0) + v_2(T(u_0))), \quad (3.34)$$

by differentiating (3.22) twice with respect to u_0 , where $v_2(t) = v''_{uu}(t, u_0)$ satisfies $v_2(0) = 0$ and

$$\dot{v}_2 = -kv^{-k-1}v_2 + k(k+1)v^{-k-2}v_1^2.$$

Since $\dot{v}_1(0) = 2$ and $v_1(t) > 0$, it follows that $v_2(t) > 0$ for all $t > 0$. Consequently, by the first property in (3.21), (3.34) gives $T''(u_0) < 0$, proving the last property in (3.21). \square

Fixing the domains, we can apply regular perturbation theory to conclude that (3.21) also holds for all $0 < \epsilon \ll 1$. In combination, this proves (ii) in Theorem 1.1(d).

To prove (i) in Theorem 1.1(d), we sketch the argument as follows. First, we work in chart $(\bar{\rho} = 1)_1$ near p_L using the coordinates in Lemma 3.4. We then describe a mapping from $\Sigma_L^{\text{in}, L}$, consisting of all those points in Σ_L^{in} with $x_1 < -c^{-1}\epsilon_1^{2k/(2k+1)}$, recall (3.12), to the section

$$\Sigma_L^{\text{out}, L} = \{(\rho_1, x_1, \epsilon_1) | x_1 = -\nu, \rho_1 \in [0, \beta_1], \epsilon_1 \in [0, \beta_2]\}.$$

This gives an expanding map, but as before, this expansion is compensated by the contraction eventually gained at p_R . Essentially, the result therefore follows from the details of the mapping from $\Sigma_L^{\text{out}, L}$ to $\Sigma_R^{\text{in}, C}$. This mapping can be described in

two parts. The first part consists of a simple, near-identity mapping, near $(\bar{\rho}, \bar{x}, \bar{\epsilon}) = (0, -1, 0)$, which can be studied in the chart $\bar{x} = -1$, the details of which are standard and left out of this manuscript completely for simplicity. The second part, is described in $(\bar{\epsilon} = 1)_2$ using the local dynamics near the nonhyperbolic saddle p_a . This mapping is contracting due to the exponential contraction towards the center manifold that extends the invariant manifold S_ϵ onto the blowup sphere. In combination, this then proves (i).

(iii) in Theorem 1.1(d) is simpler and can be described in the chart $(\bar{\rho} = 1)_1$ only. For this we compose Q as a mapping, using the coordinates in Lemma 3.4, from $\Sigma_L^{\text{in}, R}$, consisting of all those points in Σ_L^{in} with $x_1 > c^{-1}\epsilon_1^{2k/(2k+1)}$, to

$$\Sigma_L^{\text{out}, R} = \{(\rho_1, x_1, \epsilon_1) | x_1 = \nu, \rho_1 \in [0, \beta_1], \epsilon_1 \in [0, \beta_2]\}.$$

subsequently followed by a map from $\Sigma_L^{\text{out}, R}$ to

$$\Sigma_R^{\text{in}, L} = \{(\rho_1, x_1, \epsilon_1) | x_1 = -\nu, \rho_1 \in [0, \beta_1], \epsilon_1 \in [0, \beta_2]\},$$

using the transformed coordinates near p_R , see (3.13), and lastly by a mapping from $\Sigma_R^{\text{in}, L}$ to Σ_R^{out} . As before, the first mapping is expanding but this is compensated by the same contraction of the last mapping. By adjusting the domains, the mapping from $\Sigma_L^{\text{out}, R}$ to $\Sigma_R^{\text{in}, L}$ is also near-identity due to the invariance of the x_1 -axis. In combination, this proves (iii) and the proof Theorem 1.1. In particular, we highlight that domains of (i) and (ii) as well as of (ii) and (iii) can be chosen to overlap.

4. PROOF OF THEOREM 1.4

The periodic orbits we describe are fix points of $P(\cdot, \epsilon, \alpha)$. Using (1.9), we write the fix point equation as

$$Q(x, \epsilon, \alpha) = R^{-1}(x, \epsilon, \alpha),$$

where $R^{-1}(\cdot, \epsilon, \alpha) : I_R \rightarrow I_L$ is the inverse $R(\cdot, \epsilon, \alpha)$. Combining Theorem 1.1(d) and Lemma 1.3, we obtain the diagram in Fig. 10 for the graphs of $Q(\cdot, \epsilon, \alpha)$ and $R^{-1}(\cdot, \epsilon, \alpha)$ for ϵ and α sufficiently small. Notice, by (1.11) that the slope of R^{-1} is greater than $-1 + \omega$, say, for some (new) fixed $\omega > 0$, and by (1.12) that the effect of varying α is basically to translate R^{-1} vertically, keeping Q fixed. In particular, it follows that upon decreasing α in Fig. 10, the graphs of Q and R^{-1} will eventually intersect. Furthermore, by continuity and monotonicity there exists an α for which one single intersection exists. The monotonicity of R^{-1} with respect to α also shows that that this value is unique and occurs within the domain (ii) of Theorem 1.1(d). Hence it corresponds to a unique quadratic tangency $\mathcal{O}(\epsilon^{2k/(2k+1)})$ -close to γ_L . Finally Lemma 1.3, in particular (1.12), together with the implicit function theorem, implies that $\alpha = \epsilon^{2k/(2k+1)}n(\epsilon)$ as claimed.

5. DISCUSSION

Comparison with previous results. [2] also describes the regularization of the visible fold, but only for the class of regularizations in (1.7). They also assume an algebraic condition like (A2) but at $s = \pm 1$ rather than asymptotically. [2, Theorem 2.2] describes the invariant manifold's intersection with a fixed section, similar to Theorem 1.1(b). For their regularization functions, $m(\epsilon) = \gamma_L + \mathcal{O}(\epsilon)$ to leading order for any k . In [19, Theorem 3.3] this result was rediscovered using blowup. This allowed for a more detailed expression of the remainder.

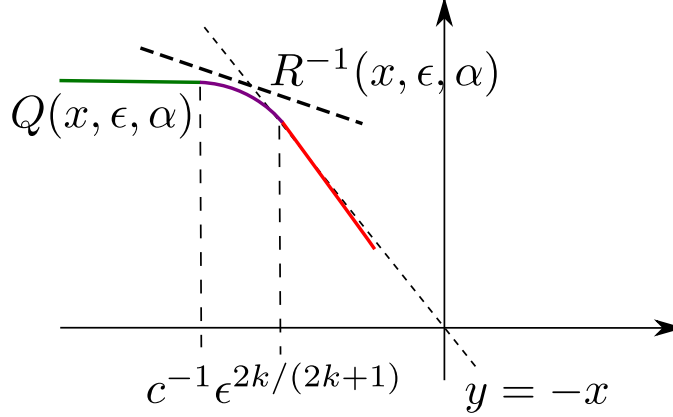


FIGURE 10. Graphs of Q (thick curve in different colours) and R^{-1} (thin dotted line), following Theorem 1.1(d) and Lemma 1.3. The different colours on the graph of Q , represents the different domains in Theorem 1.1(d): Green for domain in (i), purple for domain in (ii), red for domain in (iii). By Lemma 1.3, a quadratic tangency between these graphs occur within the purple domain, upon adjusting α . This tangency is the saddle-node bifurcation of limit cycles.

[2, Theorem 2.3] also addresses the grazing bifurcation, described in the present manuscript in Theorem 1.4, but [2] did not rigorously establish existence nor uniqueness of a saddle-node bifurcation. Our results improve on these results in several ways. Firstly, we provide more details close to the tangency, see Theorem 1.1(d), for a more general, and more practical, class of regularization functions. In turn, this allowed us to prove the existence and uniqueness of a saddle-node bifurcation in the regularized grazing bifurcation. Interestingly, in [2], the equation $y'(x) = x + y^k$, where k is the order of the tangency at $s = 1$, recall (1.7), plays an important role. For our regularization functions, satisfying (A1)-(A2), this equation is replaced by a Chini equation, see (3.19). It is essentially the analysis of this equation in Section 3.4, along with the special linearization technique used in Section 3.1 near the hyperbolic points p_L and p_R , recall Lemma 3.4, that allows us to obtain our results.

Regularization functions. In this paper, we have considered a wide class of regularization functions. However, it may seem restrictive that (1.4) holds for all ϵ . But if

$$\phi(y_2, \epsilon) \rightarrow \begin{cases} b(\epsilon) & \text{for } y_2 \rightarrow \infty, \\ a(\epsilon) & \text{for } y_2 \rightarrow -\infty, \end{cases} \quad (5.1)$$

for example, with $a(0) < b(0)$, then

$$\tilde{\phi}(y_2, \epsilon) = \frac{\phi(y_2, \epsilon) - a(\epsilon)}{b(\epsilon) - a(\epsilon)}.$$

satisfies (1.4). We can then write $Z(z, \phi, \alpha) = \tilde{Z}(z, \tilde{\phi}, \epsilon, \alpha)$ and subsequently \tilde{Z} in the form (1.2). Notice, that following this procedure \tilde{Z}_{\pm} will in general depend

upon ϵ . However, only to keep the notation as simple as possible, we focused on the simpler setting in (1.2).

The class of functions include standard regularization functions, such as $\arctan(y/\epsilon)$, $y/\sqrt{y^2 + \epsilon^2}$, but also nontrivial ones like the Goldbeter-Koshland function:

$$\phi(s, \epsilon) = \frac{\epsilon^2 s + \epsilon \sqrt{\epsilon^2 s^2 + 2\epsilon s^2 + 4\epsilon s + s^2 + 4} + 2\epsilon + \epsilon s + 2}{(\epsilon + 1)(\epsilon s + \sqrt{\epsilon^2 s^2 + 2\epsilon s^2 + 4\epsilon s + s^2 + 4} - s + 2)}.$$

This function appears as a steady-state solution for a two-state biological system, see [10]. It therefore appears naturally in QSS approximations and for ϵ small, which in biological contexts is given in terms of rate constants, it is switch-like. In fact, I have here normalised the function such that

$$\phi(y\epsilon^{-1}, \epsilon) \rightarrow \begin{cases} 1 & \text{for } y > 0, \\ 0 & \text{for } y < 0, \end{cases}$$

for $\epsilon \rightarrow 0^+$. Notice that

$$\phi(s, 0) = \frac{2}{2 - s + \sqrt{s^2 + 4}},$$

where $k_{\pm} = 1$. Functions like $\tanh(y/\epsilon)$, where $k_{\pm} = \infty$ in (A2), are more difficult, because the blowup method does not apply directly, but they can, at least when the remainder is exponential, be tackled using the technique in [19], see e.g. [19, Theorem 3.5].

If the regularization function ϕ is not monotone, such that (A1) and (1.3) are not satisfied, then the critical manifold \bar{S} upon blowup, will have folds, where, working in the scaling chart $(\bar{\epsilon} = 1)_2$, see (A.1), classical results from singular perturbation theory can be applied, e.g. [23] or canard theory [24]. ($\phi(s, \epsilon) = s/\sqrt{s^2 + \epsilon s + 1}$ is an example with a fold $s = -2\epsilon^{-1} \rightarrow -\infty$ for $\epsilon \rightarrow 0$. In such cases, additional blowups are probably required to resolve such phenomena.) See also [3] for an application; in these cases Filippov does not agree with the $\epsilon \rightarrow 0$ limit. Similarly, if (A0) does not hold, then the scaling chart, obtained by setting $y = \epsilon y_2$, is simply a general slow-fast system; it can be as complicated as a planar slow-fast system can be and there is little value in making the PWS connection.

The friction oscillator: The $\alpha = 0$ case. In the friction oscillator problem, considered in Section 2, there is another bifurcation when $\alpha = 0$ for the PWS system where the equilibrium within $y > 0$ intersects the switching manifold. For relevant parameters, the equilibrium is an unstable focus of Z_+ at $\alpha = 0$. In the PWS literature, see e.g. [25], this bifurcation is known as a boundary focus and for $0 < \epsilon \ll 1$ it gives rise to an additional Hopf bifurcation, where numerical computations suggest that the limit cycles, studied in Section 2, terminate. In [13], the authors pursue a rigorous proof of this using blowup. The bifurcation is highly degenerate since the slow flow on the invariant manifold, recall Theorem 1.1(a), vanishes for $\alpha = 0$.

ACKNOWLEDGEMENT

The author would like to thank Samuel Jelbart for bringing the friction oscillator and the model (2.5) to my attention, for sharing references on the subject and for providing valuable feedback on an earlier version of the manuscript.

APPENDIX A. PROOF OF THEOREM 1.1(A)

The analysis in the chart $\bar{y} = -1$, see (3.1), plays little role and is similar to how we deal with $\bar{y} = 1$. The details are therefore omitted. In the following we therefore consider $\bar{\epsilon} = 1$ and $\bar{y} = 1$ only.

A.1. **Chart $\bar{\epsilon} = 1$.** In this chart, we obtain the following equations

$$\begin{aligned}\dot{x} &= \epsilon\phi(y_2, \epsilon)(1 + f(x, \epsilon y_2)), \\ \dot{y}_2 &= \phi(y_2, \epsilon)(2x + \epsilon y_2 g(x, \epsilon y_2)) + 1 - \phi(y_2, \epsilon),\end{aligned}\tag{A.1}$$

using (1.6). This is a slow-fast system with x slow and y_2 fast. Setting $\epsilon = 0$ gives the layer problem where x is a parameter and

$$\dot{y}_2 = \phi(y_2, 0)2x + 1 - \phi(y_2, 0),$$

and hence a normally hyperbolic and attracting, but noncompact, critical manifold:

$$S = \{(x, y_2) \in U_\xi \mid \phi(y_2, 0) = \frac{1}{1 - 2x}, x < 0\}.\tag{A.2}$$

Fixing $J = [-\xi, -\nu]$, we can apply Fenichel's theory to $S \cap \{x \in J\}$ and conclude the existence of the invariant manifold S_ϵ in Theorem 1.1(a). The fact that $Z|_{S_\epsilon}$ is a regular perturbation of the Filippov vector-field is standard and follows easily from the fact that the reduced problem on S :

$$x' = \phi(y_2, 0)(1 + f(x, 0)) = \frac{1}{1 - 2x}(1 + f(x, 0)),$$

coincides with Filippov.

A.2. **Chart $\bar{y} = 1$.** In this chart, we obtain the following equations

$$\begin{aligned}\dot{r}_1 &= -r_1 F(r_1, x, \epsilon_1), \\ \dot{x} &= r_1(1 - \epsilon_1^k \phi_1(r_1, \epsilon_1))(1 + f(x, r_1)), \\ \dot{\epsilon}_1 &= \epsilon_1 F(r_1, x, \epsilon_1),\end{aligned}$$

where

$$F(r_1, x, \epsilon_1) = -(1 - \epsilon_1^k \phi_1(r_1, \epsilon_1))(2x + r_1 g(x, r_1)) - \epsilon_1^k \phi_1(r_1, \epsilon_1),$$

using (1.6) and (3.1). Focus first on $x \in J$. Then for $r_1 \geq 0$ and $\epsilon_1 \geq 0$ but sufficiently small we have $F > 0$ and hence the system is topological equivalent with the following version

$$\begin{aligned}\dot{r}_1 &= -r_1, \\ \dot{x} &= r_1(1 - \epsilon_1^k \phi_1(r_1, \epsilon_1)) \frac{(1 + f(x, r_1))}{F(r_1, x, \epsilon_1)}, \\ \dot{\epsilon}_1 &= \epsilon_1,\end{aligned}\tag{A.3}$$

The set $r_1 = \epsilon_1 = 0$ is therefore a line of equilibria having stable and unstable manifolds contained within $\epsilon_1 = 0$ and $r_1 = 0$, respectively. We can straighten out the individual unstable manifolds of points on $x \in J$, $r_1 = \epsilon_1 = 0$ by a transformation

of the form $\tilde{x} \mapsto x = m(\tilde{x}, r_1)$, $r_1 \in [0, \xi]$ with m smooth, with $m'_x > 0$. Applying this transformation to (A.3) gives

$$\begin{aligned}\dot{r}_1 &= -r_1, \\ \dot{x} &= \epsilon G(r_1, x, \epsilon_1), \\ \dot{\epsilon}_1 &= \epsilon_1,\end{aligned}$$

dropping the tilde on x . Recall here that $\epsilon = r_1 \epsilon_1$. Therefore if we consider an initial condition with $r_1(0) = \delta > 0$ small, then

$$\begin{aligned}r_1(t) &= e^{-t}\delta, \\ x(t) &= x(0) + \mathcal{O}(\epsilon t), \\ \epsilon_1(t) &= e^t \epsilon_1(0).\end{aligned}\tag{A.4}$$

Now, we wish to extend the stable foliation of S_ϵ by the backward flow. For this let $x \in J$, after possibly decreasing $\nu > 0$ and ξ , and consider the leaf $\mathcal{F}_{x,\epsilon}$ of the Fenichel foliation of S_ϵ . We therefore flow this set forward $t = \mathcal{O}(\log \epsilon^{-1})$, which is the time it takes for r_1 to go from $\mathcal{O}(1)$ to $\mathcal{O}(\epsilon)$. This gives a new x , $x' = x \cdot t$, say, and a new leaf $\mathcal{F}_{x',\epsilon}$. Notice $\phi_t(\mathcal{F}_{x,\epsilon}) \subset \mathcal{F}_{x',\epsilon}$ and hence we extend $\mathcal{F}_{x,\epsilon}$ by flowing $\mathcal{F}_{x',\epsilon}$ backwards by time t . (In general, $\mathcal{F}_{x',\epsilon}$ will not be fully covered by the chart $\bar{y} = 1$ and therefore we will have to work in separate charts.) We do this by using (A.4), which produces the extended leafs as images of Lipschitz mappings.

REFERENCES

- [1] E. J. Berger. Friction modeling for dynamic system simulation. *Applied Mechanics Reviews*, 55(6):535–577, 2002.
- [2] C. Bonet-Revés and T. M-Seara. Regularization of sliding global bifurcations derived from the local fold singularity of Filippov systems. *Discrete and Continuous Dynamical Systems-Series a*, 36(7):3545–3601, 2016.
- [3] E. Bossolini, M. Brøns, and K. U. Kristiansen. Singular limit analysis of a model for earthquake faulting. *Nonlinearity*, 30(7):2805–2834, 2017.
- [4] M. Desroches and M. R. Jeffrey. Canards and curvature: nonsmooth approximation by pinching. *Nonlinearity*, 24(5):1655–1682, May 2011.
- [5] M. di Bernardo, C. J. Budd, A. R. Champneys, and P. Kowalczyk. *Piecewise-smooth Dynamical Systems: Theory and Applications*. Springer Verlag, 2008.
- [6] F. Dumortier and R. Roussarie. Canard cycles and center manifolds. *Mem. Amer. Math. Soc.*, 121:1–96, 1996.
- [7] N. Fenichel. Persistence and smoothness of invariant manifolds for flows. *Indiana University Mathematics Journal*, 21:193–226, 1971.
- [8] N. Fenichel. Asymptotic stability with rate conditions. *Indiana University Mathematics Journal*, 23:1109–1137, 1974.
- [9] N. Fenichel. Geometric singular perturbation theory for ordinary differential equations. *J. Diff. Eq.*, 31:53–98, 1979.
- [10] A. Goldbeter and D. E. Koshland. An amplified sensitivity arising from covalent modification in biological systems. *Proceedings of the National Academy of Sciences*, 78(11):6840–6844, 1981.
- [11] N. Guglielmi and E. Hairer. Classification of hidden dynamics in discontinuous dynamical systems. *Siam Journal on Applied Dynamical Systems*, 14(3):1454–1477, 2015.
- [12] F. Heslot, T. Baumberger, B. Perrin, B. Caroli, and C. Caroli. Creep, stick-slip, and dry-friction dynamics - experiments and a heuristic model. *Physical Review E*, 49(6):4973–4988, 1994.
- [13] S. Jelbart, M. Wechselberger, and K. U. Kristiansen. The boundary focus in the friction oscillator problem. *in preparation*, 2019.
- [14] C.K.R.T. Jones. *Geometric Singular Perturbation Theory, Lecture Notes in Mathematics, Dynamical Systems (Montecatini Terme)*. Springer, Berlin, 1995.

- [15] P. Kaklamanos and K. U. Kristiansen. Regularization and geometry of piecewise smooth systems with intersecting discontinuity sets. *Siam Journal on Applied Dynamical Systems*, 18(3):1225–1264, 2019.
- [16] I. Kosiuk and P. Szmolyan. Geometric singular perturbation analysis of an autocatalator model. *Discrete and Continuous Dynamical Systems - Series S*, 2(4):783–806, 2009.
- [17] I. Kosiuk and P. Szmolyan. Scaling in singular perturbation problems: Blowing up a relaxation oscillator. *Siam Journal on Applied Dynamical Systems*, *Siam J. Appl. Dyn. Syst*, *Siam J a Dy*, *Siam J Appl Dyn Syst*, *Siam Stud Appl Math*, 10(4):1307–1343, 2011.
- [18] I. Kosiuk and P. Szmolyan. Geometric analysis of the Goldbeter minimal model for the embryonic cell cycle. *Journal of Mathematical Biology*, *J. Math. Biol*, *J Math Biol*, 2015.
- [19] K. U. Kristiansen. Blowup for flat slow manifolds. *Nonlinearity*, 30(5):2138–2184, 2017.
- [20] K. Uldall Kristiansen and S. J. Hogan. On the use of blowup to study regularizations of singularities of piecewise smooth dynamical systems in \mathbb{R}^3 . *SIAM Journal on Applied Dynamical Systems*, 14(1):382–422, 2015.
- [21] K. Uldall Kristiansen and S. J. Hogan. Regularizations of two-fold bifurcations in planar piecewise smooth systems using blowup. *SIAM Journal on Applied Dynamical Systems*, 14(4):1731–1786, 2015.
- [22] K. Uldall Kristiansen and S. J. Hogan. Resolution of the piecewise smooth visible-invisible two-fold singularity in \mathbb{R}^3 using regularization and blowup. *Journal of Nonlinear Science*, 29(2):723–787, 2018.
- [23] M. Krupa and P. Szmolyan. Extending geometric singular perturbation theory to nonhyperbolic points - fold and canard points in two dimensions. *SIAM Journal on Mathematical Analysis*, 33(2):286–314, 2001.
- [24] M. Krupa and P. Szmolyan. Relaxation oscillation and canard explosion. *Journal of Differential Equations*, 174(2):312–368, 2001.
- [25] Yu. A. Kuznetsov, S. Rinaldi, and A. Gragnani. One parameter bifurcations in planar Filippov systems. *Int. J. Bif. Chaos*, 13:2157–2188, 2003.
- [26] J. Llibre, P. R. da Silva, and M. A. Teixeira. Regularization of discontinuous vector fields on \mathbb{R}^3 via singular perturbation. *J. Dyn. Diff. Eq.*, 19:309–331, 1997.
- [27] O. Makarenkov and J. S. W. Lamb. Dynamics and bifurcation of nonsmooth systems: A survey. *Physica D*, 241:1826–1844, 2012.
- [28] F. W. J. Olver, D. W. Lozier, R. F. Boisvert, and C. W. Clark. Nist handbook of mathematical functions. *Journal of Geometry and Symmetry in Physics*, pages 99–104, 2011.
- [29] J. Sotomayor and M. A. Teixeira. Regularization of discontinuous vector fields. In *Proceedings of the International Conference on Differential Equations, Lisboa*, pages 207–223, 1996.
- [30] H. I. Won and J. Chung. Stickslip vibration of an oscillator with damping. *Nonlinear Dynamics*, 86(1):257–267, 2016.